ORIGINAL RESEARCH

CrossMark

Evaluation of the dynamic p–y_p loops of pile-supported structures on sloping ground

Bao Ngoc Nguyen[1] · Nghiem Xuan Tran[2] · Jin-Tae Han[3] · Sung-Ruyl Kim[2]

Abstract

A key issue in the design of pile-supported structures on sloping ground is soil–pile interaction, which becomes more complicated in case of dynamic loading. This study aimed to evaluate the effect of slope on the dynamic behavior of pile-supported structures by performing a series of centrifuge tests. Three models were prepared by varying the slope and soil density of dry sand grounds. The mass supported on 3 by 3 group piles was shaken applying sinusoidal wave with various amplitudes. Test results showed that the location of maximum values and distribution shape of the bending moment below the ground surface varied noticeably with the pile position in the slope case. The relationship between the soil resistance and pile deflection (p–y_p loops) was carefully evaluated by applying the piecewise cubic spline method to fit the measured bending moment curves along piles. It was found that the shape of the p–y_p loops was irregular due to the effect of slope, and immensely influenced by the movement of the unstable zone. In addition, the effect of the pile group in the horizontal case was evaluated by comparing with the previously suggested curves that represent the relationship between the soil resistance and pile–soil relative displacement (p–y curves) to propose the multiplier coefficients.

Keywords Soil–pile interaction · Pile-supported wharf · Dynamic p–y curve · Sloping ground · Centrifuge test

1 Introduction

Berthing-mooring structures, such as pile-supported wharves and piers, play an important role in seaport transportation system. Such structures located near the shore work under complicated loading conditions induced by wind and ocean waves, berthing loads from

✉ Sung-Ruyl Kim
  sungryul@snu.ac.kr

1   Department of Civil Engineering, Dong-A University, 840 Hadan2-dong, Saha-gu, Busan, South Korea

2   Department of Civil and Environmental Engineering, Seoul National University, 1 Gwanak-ro, Gwanak-gu, Seoul, South Korea

3   Earthquake Safety Research Division, Korea Institute of Civil Engineering and Building Engineering Technology, 283, Goyang-daero, Ilsanseo-gu, Goyang-si, Gyeonggi-do, South Korea

vessels, and even seismic loads. Selection and evaluation of suitable foundation types for these structures pose a challenge for civil engineers because they are usually subjected to large loads and are occasionally built on soft slope grounds. Pile foundations are the most effective solutions by which large loads are transmitted from the surface to a strong bearing stratum.

In relation to the design of the pile foundation, lateral soil–pile interaction is a major concern. The most popular and effective approach for soil–pile interaction simulation is based on the theory of a beam on a nonlinear Winkler foundation. In this model, the resistance of the supporting ground is represented by a set of discrete nonlinear springs. The lateral pile–soil interaction is characterized by pile deflection (y_p) and lateral soil resistance (p) acting on each segment along the pile.

Over the past decades, p–y_p curves have been proposed based on field experiments or model tests. The p–y_p curve was initially developed by performing field loading tests and laboratory tests on small-diameter piles under static and cyclic loading conditions (Matlock 1970; Reese et al. 1974; Murchinson and O'Neill 1984; Georgiadis et al. 1992). The p–y_p curve was then extended to consider the dynamic behavior of piles under seismic loading. Based on the dynamic centrifuge test results or the dynamic field tests, several researchers proposed rigorous analytical models consisting of p–y springs and dashpots (Nogami et al. 1992; El Naggar and Novak 1995; Boulanger et al. 1999; El Naggar and Bentley 2000; Gerolymos and Gazetas 2005; Gerolymos et al. 2009; Rovithis et al. 2009; Varun 2010). These models still used previously suggested p–y_p curves of static condition.

However, the behavior of "seismic" or "dynamic" p–y_p curves has not been thoroughly understood. Yoo et al. (2013) performed centrifuge tests to determine the parameters of dynamic p–y backbone curves for pile foundations in dry sand (where y is the relative displacement between soil and pile). Results showed that the stiffness of dynamic p–y curves decreased with increasing amplitude of input motions. The authors also claimed that the pseudo-static analysis with the static p–y_p curve from API (2000) gave an overestimation of the maximum bending moment and pile displacement. Choi et al. (2015) developed another p–y curve using bounding surface plasticity theory. The p–y curve was then implemented in a finite element program to simulate the behavior of pile foundations in sand under seismic loading.

All tests mentioned above were conducted for pile foundations in level ground. For pile-supported structures on sloping ground, such as pile-supported wharves and piers, the slope effects on the behavior of p–y curves become significant. Mezazigh and Levacher (1998) conducted centrifuge tests to investigate the effects of slopes on p–y_p curves for a single pile in dry sand. The single pile was located on the horizontal surface near the slope crest. The authors found that the displacement and maximum bending moment of the pile near the slope crest increased. Moreover, the stiffness and lateral soil resistance of p–y_p curves were significantly reduced. Muthukkumaran et al. (2008) performed 1-g model tests of single piles in dry sand to formulate the p–y_p curves considering the slope effect. The single pile was installed at the crest of the slope. The authors reaffirmed the findings of Mezazigh and Lavacher. However, all previous tests for the piles in slope were performed under static conditions and no studies have been conducted about the dynamic p–y curves of a pile in a slope.

In addition, several pile-supported wharves in slope were substantially damaged under strong earthquake during a past decade, e.g. the Great Hanshin (Kobe) earthquake in 1995; the Haiti earthquake at Port-au-Prince in 2010. Lessons from these events have been considered in several design codes (OCDI 2009; ASCE 2014), which provide a detailed

guideline for designing the wharf structure. However, the effect of slope on the behavior of dynamic soil–pile interaction of the pile-supported wharf under seismic loading condition has not been considered in the aforementioned studies. Thus, it is important for carrying out studies to clarify this aspect.

The current study aimed to evaluate the effect of the slope on the behavior of pile-supported wharves under seismic loading. Dynamic centrifuge tests were conducted to compare the dynamic behavior of piles in horizontal and slope grounds. The model tests were carried out in both dry loose and dense sandy soil. The piecewise cubic spline method was used to fit the obtained bending moment distribution curves. Finally, the seismic behavior of piles considering slope effects was analyzed in terms of the $p–y_p$ loops derived from the bending moment distribution curves.

2 Centrifuge testing program

2.1 Centrifuge modeling

Experimental centrifuge tests were performed by using a centrifuge at Korea Advanced Institute of Science and Technology (KAIST). The centrifuge has an arm length of 5 m and the maximum centrifugal acceleration up to 240g-tons (Kim et al. 2013). All model tests reported in this study were conducted at a centrifugal acceleration of 48g. The scaling law for centrifuge modeling was adopted from Wood (2004) and Madabhushi (2014), as shown in Table 1. All data in this study are presented in prototype scale, unless stated otherwise.

Figure 1 shows the layout of centrifuge modeling, including the soil layer, structural model, and instrumentation. A pile-supported wharf located in the coastal city of Pohang, South Korea was selected for centrifuge modeling. In this study, the wharf segment had nine piles with three rows and three columns. All the piles supported a deck with a thickness of 0.960 m, and they had the same diameter of 0.912 m and a length of 24 m. The slope angle of the ground surface was about 33°. The pile foundation completely penetrated a sandy soil layer and was founded on a rock layer.

Each aluminum tubular pile, which had a 1.9 cm external diameter and a 0.1 cm wall thickness in model scale, was attached to seven pairs of strain gauges along the pile length to obtain the bending moment, as shown in Fig. 1.

Table 1 Scaling law applied for dynamic centrifuge modeling

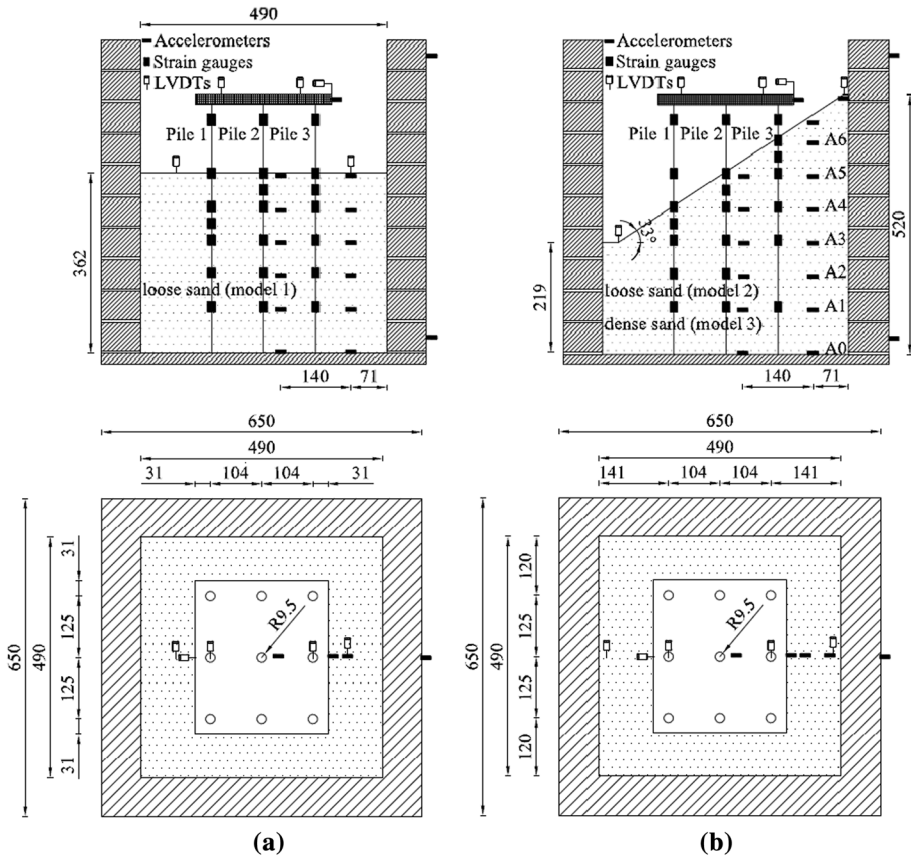| Quantities	Scaling factor (model/proto-type)	Values		Unit
		Model	Prototype	
Length	$1/N$	1	48	m
Stress	1	1	1	kN m^{-2}
Strain	1	1	1	–
Bending moment	$1/N^3$	1	110592	kN m
Time	$1/N$	1	48	s
Frequency	N	1	0.02	Hz
Acceleration	N	1	0.02	g

Fig. 1 Schematic diagram of the centrifuge test models (dimension in model scale, unit: mm). **a** Horizontal case, **b** slope case

Calibration of the model piles was performed to obtain the flexural stiffness (*EI*) of the pile. After fixing the pile toe, the pile head was loaded by suspending a mass. The bending moment of each calibration was calculated by the product of the weight applied and the moment arm. The *EI* value of the model pile was determined as about 779.3 MN m^2 in the prototype scale. All properties of model piles and deck are summarized in Table 2.

Table 2 Properties of model piles and deck

Pile properties	Model	Prototype	Unit
Outer diameter	0.019	0.912	m
Wall thickness	0.001	0.048	m
Flexural rigidity	1.468E−01	7.793E+05	kN m^2
Mass of deck	0.423E+01	4.678E+05	kg

2.2 Model preparation and testing procedure

The wharf model was prepared in an equivalent shear beam (ESB) box, which consisted of a series of rigid rings separated by soft rubber layers. The dimensions of the ESB box were 49 cm × 49 cm × 63 cm. The ESB box was designed to enable the free field movement of soil layers, thereby reducing the rigid wall effect. Lee et al. (2012) investigated the effect of the wall of the ESB box and concluded that the response of soil and container wall may be different in the case of partially filled models. In this test, the phase information of the soil and container wall accelerations showed that the boundary effect could be insignificant within the range of the single predominant frequency of 1 Hz. In addition, the structure was placed at the center of the box to minimize the effect of the container wall on the structural response. However, the boundary effect could affect the stability of the slope and seismic behavior of models.

The model was prepared through the following steps. First, the piles were fixed onto the bottom of the ESB box using an aluminum plate. Second, a uniform sandy ground was made using an air pluviation technique. Finally, the deck was rigidly attached to the pile head. The density of dry silica sands was achieved by controlling the raining height, moving speed of an automatic sand rainer, and opening diameter of the nozzle.

The three models consisted of Model 1 (horizontal layer, ground relative density of about 45%), Model 2 (sloped layer, ground relative density of about 40%) and Model 3 (sloped layer, ground relative density of about 80%).

While preparing the grounds, instruments were installed on structures or in the ground, as shown in Fig. 1. Three linear variable differential transformers (LVDTs) were used to monitor the vertical and horizontal displacements of the deck. Ground surface settlement was measured by two other LVDTs as well. An accelerometer was attached to the deck to record the inertial acceleration of the deck during shaking. In this study, the positive direction of inertial acceleration was defined as the downslope direction. Moreover, accelerometers were placed in the ground to observe the seismic response of the soil.

The spinning time of the centrifuge to reach $48g$ from 1 g was approximately 18 min. Before applying the dynamic loading, the centrifugal acceleration of $48g$ was maintained for approximately 15 min to heat the oil of the shaking table and prepare the input motions. A sinusoidal wave with 1 Hz frequency was applied at the base of the soil box and the amplitude of the wave varied from 0.1 to 0.28 g. A typical acceleration time history and Fast Fourier Transform (FFT) spectrum of the input motion are presented in Fig. 2. The detailed shaking program is listed in Table 3.
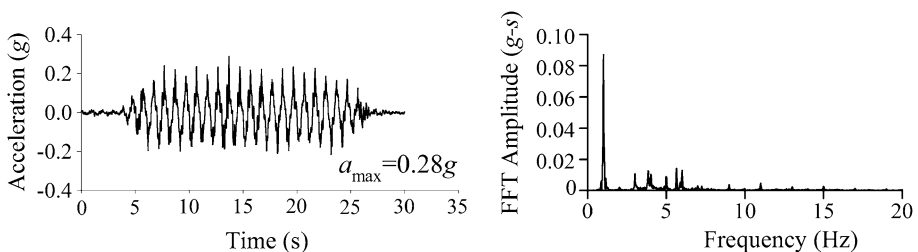

Fig. 2 Typical input motion (Model 3, $a_{base} = 0.28g$)

Table 3 Test programs

Test no.	Model ground	Input motion		
		Type	Amplitude[a] (g)	Frequency (Hz)
Model 1	Horizontal ($D_r = 45\%$)	Sinusoidal	0.1, 0.14, 0.21, 0.25	1
Model 2	Slope ($D_r = 40\%$)	Sinusoidal	0.14, 0.18, 0.24	1
Model 3	Slope ($D_r = 80\%$)	Sinusoidal	0.15, 0.22, 0.28	1

[a]Denotes values directly obtained from the raw data

3 Evaluation of p–y_p loops

3.1 Curve fitting technique

The measured strains in dynamic centrifuge tests constantly contain certain "electrical noise." Thus, the measured strain data of piles were filtered to remove insignificant portions or noise. The detailed filtering process is explained in the succeeding section. Subsequently, the bending moment values along piles $M(i)$ were obtained by converting the corresponding strain values in relation to the calibration factor. Based on simple beam theory, lateral soil resistance, p and pile deflection, y_p can be respectively obtained through double differentiation and integration of the bending distribution curves. The computed y_p represents the movement of a pile relative to the base, given that the pile toe displacement is the same as the base movement. The numerical determination of p and y_p are expressed in Eqs. (1) and (2), respectively.

$$p = \frac{d^2}{dz^2} M, \tag{1}$$

$$y_p = \iint \frac{M}{EI} dz dz, \tag{2}$$

where EI is the flexural stiffness of the pile, and z is the depth below the ground surface.

To evaluate the p and y_p values, a curve fitting technique should be applied to draw the bending moment distribution curve with depth. Many researchers have applied various fitting methods to draw the bending moment distribution curve, including the polynomial function method (Ting et al. 1987; Wilson 1998; Muthukkumaran et al. 2008; Rovithis et al. 2009; Bonab et al. 2014), the cubic-spline method (Dou and Byrne 1996; Yang et al. 2011; Yoo et al. 2013), the quartic-spline method (Georgiadis et al. 1992; Khari et al. 2014), the quintic-spline method (Mezazigh and Levacher 1998), and the method of weighted residuals (Brandenberg et al. 2005; Choi et al. 2015).

Yang and Liang (2006) compared four hypothetical numerical simulations to derive p–y curves from full-scale field tests. They found that the p–y curves from the piecewise cubic polynomial method gave the smallest error on the prediction of pile deflection. Brandenberg et al. (2010) examined the accuracy of several curve fitting methods and concluded that the method of weighted residuals and cubic-spline method outperformed the

polynomial regression method. In addition, Haiderali and Madabhushi (2016) found that the cubic-spline method was consistently accurate in deriving p–y curves in comparison with other methods. Therefore, the cubic-spline method was used in the current study to fit all the bending moment distribution curves. The following procedure was applied to evaluate the p–y_p curves.

(1) The bending moment curve above the ground surface was fitted by using the linear function.

(2) The shear force at the ground surface was calculated by differentiating the linear function of the bending moment curve obtained from Step (1).

   The cubic-spline method with the clamped boundary condition (Eqs. 8, 9) was used to fit the bending moment distribution below the ground surface. The subscript i indicates the depth location from $i = 0$ (surface) and $i = n$ (pile toe). The bending moment value at pile toe was assumed to be equal to zero (Eq. 4) because a flexible pile was employed. In addition, the assumption was supported by the negligible measurement of the bending moment near the pile toe. The continuity of the bending moment distribution is achieved by applying Eq. 5. The first and second derivatives of the cubic-spline function are defined by Eqs. 6 and 7, respectively. The boundary condition in Eq. 9 was applied by considering the shear force at the pile toe as equal to zero. These boundary conditions are in accordance with the hypothesis proposed by Dou (1991) for the dynamic tests on the end bearing piles.

$$M_i(z) = M_i + \beta_i (z - z_i) + \lambda_i (z - z_i)^2 + \kappa_i (z - z_i)^3, \tag{3}$$

$$M_i(z_i) = M_i \quad \text{for each } i = 0, 1, \ldots, n - 1; \text{ and } M_{n-1}(z_n) = 0 \text{ (moment at pile toe = 0)}, \tag{4}$$

$$M_i(z_{i+1}) = M_{i+1}(z_{i+1}) \quad \text{for each } i = 0, 1, \ldots, n - 2, \tag{5}$$

$$M_i'(z_{i+1}) = M_{i+1}'(z_{i+1}) \quad \text{for each } i = 0, 1, \ldots, n - 2, \tag{6}$$

$$M_i''(z_{i+1}) = M_{i+1}''(z_{i+1}) \quad \text{for each } i = 0, 1, \ldots, n - 2, \tag{7}$$

$$M'(z_0) = V_0 \quad \text{(shear force at surface)}, \tag{8}$$

$$M'(z_n) = 0 \quad \text{(shear force at pile toe)}, \tag{9}$$

where i = depth index where strain gauges attached on the pile; β_i, λ_i, and κ_i = coefficients of the cubic-spline function; M_i = bending moment measured at z_i; V_0 = shear force at surface; z_i = depth (z_0: surface, z_n: pile toe).

   The shear force distribution curves below the ground surface was determined by differentiating the cubic-spline function of Eq. (3).

(3) The computed shear force data were again fitted by using the cubic-spline function to satisfy the nonlinear behavior of lateral soil resistance (Brandenberg et al. 2010). The clamped boundary condition, i.e., $V'(z_o) = V'(z_n) = 0$, was also applied to satisfy the lateral soil resistance being equal to zero at the ground surface and pile toe because the pile toe was moving simultaneously with the base of the ESB box.

(4) Finally, lateral soil resistance (p) was identified by differentiating the cubic-spline function of the shear force curves of Step (3). Moreover, the pile deflection (y_p) was

obtained by double integration of the cubic-spline function of Eq. (3). During the double integration, the lateral pile deflection and pile inclination at the pile toe were applied as zero following the suggestion of Haiderali and Madabhushi (2016) because these boundary conditions were appropriate for small diameter piles (diameter below 3.8 m).

A routine was made using a commercial MATLAB program to obtain the p–y_p curves from the time histories of the measured strain values (MATLAB 2016).

3.2 Selection of filtering technique

Additional noises from several electrical devices might significantly interfere with instrumented data during dynamic centrifuge tests (Madabhushi 2014). In addition, the earthquake-loading actuator produces a higher frequency which will appear in response signals (Brennan et al. 2005). These additional signals induce considerable error during the post-processing of digital data. Several methods are available for removing or filtering the unwanted signal components from the interest signal. The most important thing in the filtering techniques is to choose the appropriate cut-off frequency.

Yang et al. (2011) and Yoo et al. (2013) used the band-pass filtering to eliminate the noise generated during centrifuge testing. This filtering method is a reasonable choice for cases with no residual strain. However, residual displacement of both the ground and the structure might occur in the present tests of piles with slope grounds.

Therefore, the applicability of filtering techniques was analyzed using the test data reported by Wilson (1998). Four centrifuge models were used in this study to investigate the seismic behavior of piles. The data of piles in liquefiable grounds were selected to analyze the effect of filtering techniques on the calculation of the residual displacement (Csp2 model, event F). The LVDTs measurements were adjusted considering the relative movement of the base and the top ring of the soil box, where the LVDTs were attached.

Figure 3 shows the comparison of the pile head displacements relative to the base of the soil box obtained from strain data and from LVDTs. The displacement of the pile head calculated using the low-pass filtering showed good agreement with that obtained from LVDTs. By contrast, calculation using the band-pass filtering was unable to reproduce the residual displacement of the pile head. In addition, this comparison showed that the method used in the present study was excellent for calculating pile head displacement, thereby verifying the accuracy of the algorithm implemented in the MATLAB program as
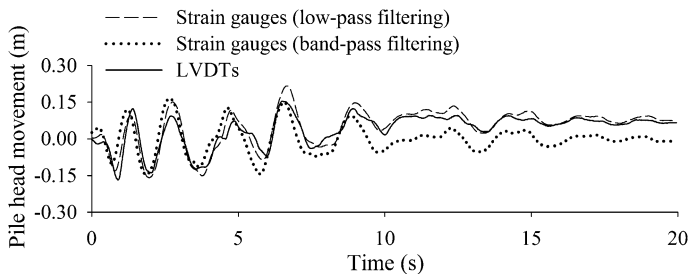

Fig. 3 Effect of filtering techniques on the calculation of pile head displacement from bending moment distribution. Data adopted from Wilson (1998)
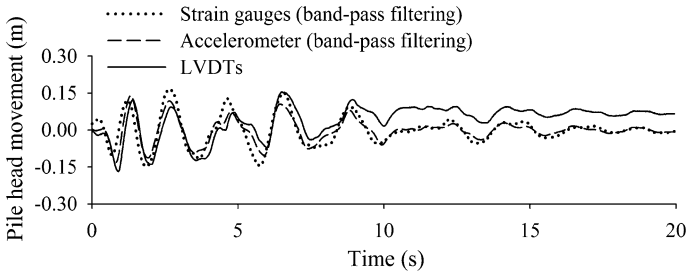
Fig. 4 Comparison of pile head displacements calculated from bending moment distribution and acceleration using band-pass filtering. Data adopted from Wilson (1998)
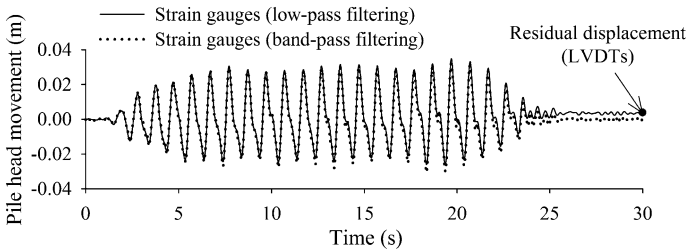

Fig. 5 Effect of filtering techniques on the calculation of pile head displacement in this study (Model 2, $a_{base} = 0.24$g)

well. Additionally, Fig. 4 presents the comparison of the pile head displacement derived from the bending moment distribution and from acceleration using the band-pass filtering method and LVDTs. Note that the residual displacement might not be achieved by both calculations.

For a further demonstration, the horizontal movement of the deck of Model 2 (sloped layer with loose sand) with a base acceleration amplitude (a_{base}) of $0.24g$ was derived from the bending moment distribution using the low-pass filtering and the band-pass filtering methods, as shown in Fig. 5. The deck movement calculated by both methods had a similar behavior in phase. However, calculation using the band-pass filtering technique could not capture the residual displacement of the deck as expected.

From the comparison above, the low-pass filtering method is appropriate for cases with residual strain, which may occur in the sloped layer in the present tests.

4 Results and analyses

4.1 Bending moment of piles

Figure 6 shows the maximum bending moment curves in the Model 1 case (horizontal layer). The strain data in Pile 3 were not analyzed due to some error in the tests. However, it was believed that the outer piles (Piles 1 and 3) showed almost similar behavior, likely due to the symmetric pile condition of the tests. The bending moment in the pile increased with the increase of the amplitude in the base acceleration. The bending moment reached

Fig. 6 Maximum bending moment distribution curves fitted by the cubic spline method (Model 1). **a** Pile 1, **b** Pile 2
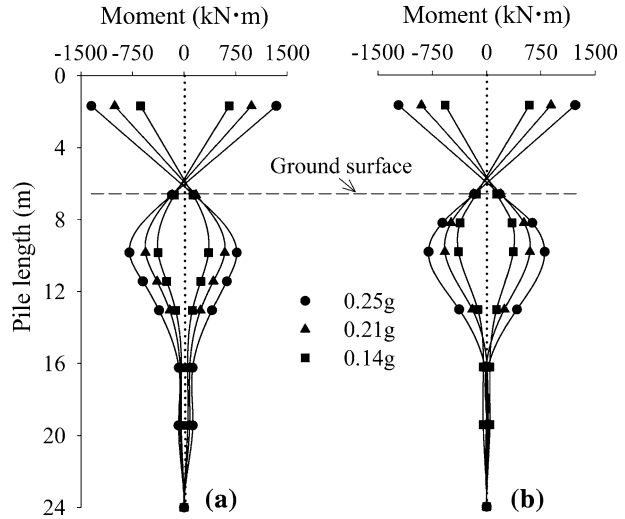
maximum at the pile head because the pile head rotation was restrained by the deck connection. Acceleration at the pile head of the center pile showed almost similar response with the deck acceleration, which was attached at one side of the deck. This result confirmed that the deck displaced horizontally instead of rotating. The bending moment below ground surface reached maximum at the depth of about $2.7D$–$3.5D$.

Figures 7 and 8 indicate the maximum bending moment curves in the cases of Models 2 and 3, respectively. In the case of the small amplitude of the input motion, the maximum bending moment below the ground surface showed similar behavior. The difference of maximum bending values between the Model 2 ($a_{base} = 0.14g$) and Model 3 ($a_{base} = 0.15g$)
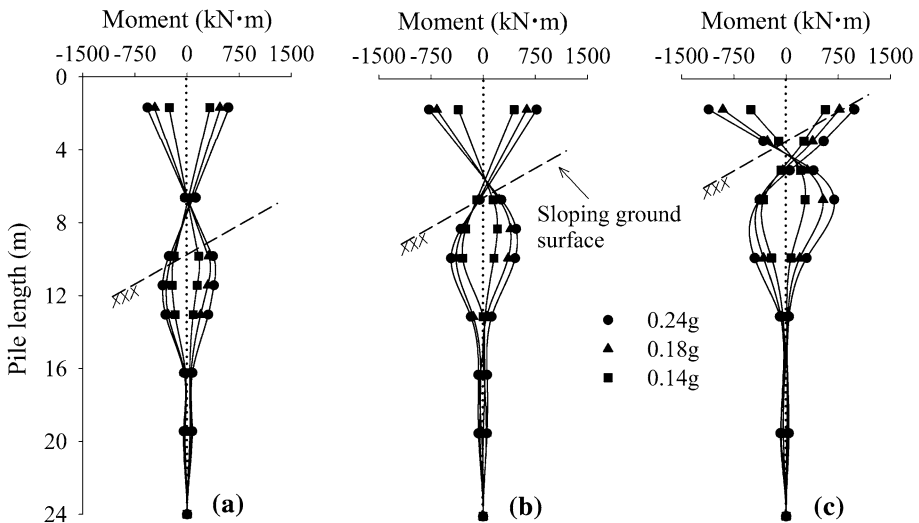

Fig. 7 Maximum bending moment distribution curves fitted by the cubic spline method (Model 2). **a** Pile 1, **b** Pile 2, **c** Pile 3
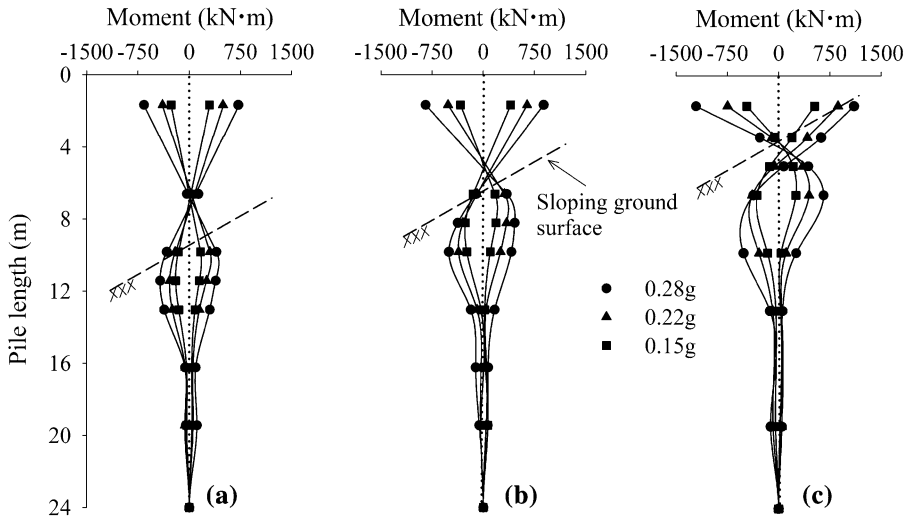
Fig. 8 Maximum bending moment distribution curves fitted by the cubic spline method (Model 3). **a** Pile 1, **b** Pile 2, **c** Pile 3

was smaller than 10%. Kwon (2014) also found that peak bending moments of a single pile in dry sand with different relative densities present a similar pattern. This finding means that the piles might be mainly affected by the contribution of inertial force induced by the mass of the superstructure. However, the difference became significant at larger amplitude of input motion. The maximum bending moment values below ground surface of Model 2 ($a_{base}=0.24g$) was larger than that of Model 3 ($a_{base}=0.22g$) by about 20–30%.

The peak displacement profiles of the soil and the deck were computed to analyze the effect of the relative density on the soil–pile–deck response (see Fig. 9). The peak displacements were calculated by the double integration of the measured acceleration and normalized by dividing the peak displacement of the base of the soil box. The difference of the soil deformation between Models 2 and 3 was less than 3% at the small amplitudes (see Fig. 9a) and about 11% at large amplitudes (see Fig. 9b) of the input motions. Evidently, the effect of the relative density on the soil–pile–deck response became larger with the increased amplitude of the input motions. Such disparity might be caused by soil deformation of the slope, which was affected significantly by the relative densities when the large amplitude of the input motion was applied.

Apparent differences were observed in the moment results between the slope and horizontal cases. For the horizontal case (Model 1), the bending moment distributions were almost symmetric regardless of shaking direction (Fig. 6). On the contrary, Figs. 7 and 8 indicate that the shape and the magnitude of the bending moment of the slope cases (Models 2 and 3) were considerably dependent on the shaking direction.

The actual location of the maximum bending moment below ground surface might occur between two measured points according to the distribution of the strain gauges along the pile. Therefore, to minimize the prediction error of the depth of the maximum bending moment, the cubic spline method was applied to draw the bending moment curve. The depth of the maximum bending moment below ground surface in the downslope direction was deeper than that in the upslope direction by 1.3–3.3 times (Model 2) and from 1.4 to 3.6 times (Model 3). The different depth of the maximum bending moment might
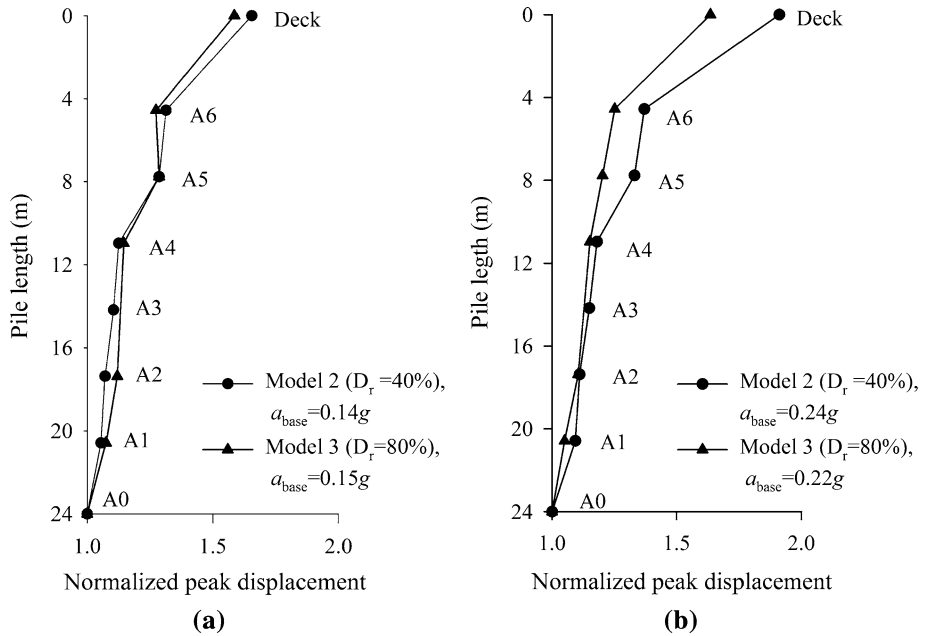
Fig. 9 Normalized peak displacement of the soil and deck with different input motions. **a** Small amplitude, **b** large amplitude

occur because the passive soil resistance against the upslope pile movement was larger than that against the downslope pile movement. In addition, the depth of the maximum moment was significantly changed according to the position of piles. For example, Fig. 7 presents that the depth of the maximum moment in Model 2 ($a_{base} = 0.24g$ and positive direction of inertial acceleration) was about 2.1D, 3.6D, and 5.4D for Piles 1, 2, and 3, respectively. Although the boundary effect of the ESB box had certain influence on the depth of the maximum bending moment, these results are consistent with the finding for the single pile installed in the sloping ground under static loading condition reported by Mezazigh and Levacher (1998) and Sivapriya and Gandhi (2011). Pile 3 had the largest embedded length. Consequently, the largest kinematic force caused by the lateral soil movement during shaking, which led to the largest moment and the deeper depth of the maximum moment on Pile 3 is located near the slope crest.

4.2 Dynamic p–y_p loops

The experimental dynamic p–y_p loops can be characterized by two parameters, namely, the stiffness and peak point of the p–y_p loops. The stiffness of the p–y_p loops is defined as the slope of the line between the origin and peak points. In case of the Model 1, Fig. 10 shows that the stiffness and the peak lateral soil resistance of the p–y_p loops increased with depth according to the increase of the confining stress. Moreover, the stiffness and peak points of the p–y_p loops of Model 1 were almost similar for both sides of piles.

In case of the models with slope, Figs. 11 and 12 indicate that the peak points of the p–y_p loops in the upslope side were much larger than those in the downslope side. By
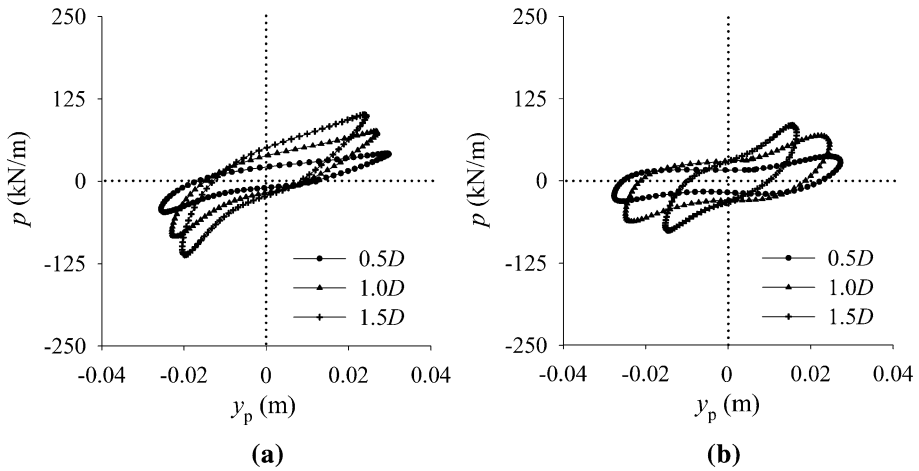
Fig. 10 Experimental dynamic p–y_p loops at various depths (Model 1, $a_{base} = 0.25g$). **a** Pile 1, **b** Pile 2

contrast, the stiffness of the p–y_p loops in the downslope side was smaller than those in the upslope side. As mentioned, the difference in earth pressure in both sides of the pile installed on the slope might have a significant effect on the p–y_p loops. It means that a larger soil reaction would resist pile movement in the positive direction due to a larger passive earth pressure.

Figure 13 depicts the behavior of p–y_p loops according to the pile position at a depth of 1.5D with the largest applied motions. Figure 13a presents that, for Model 1, the stiffness of p–y_p loops of Pile 1 was a little larger than that of Pile 2. The change of stiffness in the horizontal case might be due to the effect of the pile group, but such change was not pronounced. By contrast, the pile deflection in the slope case (Models 2 and 3) decreased noticeably from Pile 3 to Pile 1, as shown in Figs. 13b, c. Consequently, the p–y_p loops became stiffer from the crest to the toe of the slope. The behavior of Pile 1 with the largest unsupported length might be mainly governed by the inertial force component during shaking. This phenomenon is consistent with the observed behavior of the bending moment. A common shape of p–y_p loops was presented in Fig. 14 for the pile installed in the horizontal ground. Lateral soil resistance was proportioned to the increase of y_p, which means that the peak points of p–y_p loops could be found at the first and third quadrants in the graph.

Slope effect on p–y_p loops can be described in detail by comparing the full set of p–y_p loops during shaking for both horizontal and slope cases, especially at a shallow depth, as shown in Fig. 15. The positive peak point remained in the first quadrant, but the negative peak point changed from the third quadrant to the second quadrant. In the slope case, when the system moved in the downslope direction, the soil flow seemed faster than the movement of the pile through which an additional kinematic soil force acted on the piles. This phenomenon was not observed at the deeper depth and area near Pile 1 because the soil mass became more stable. The boundary effect of the container might also have an influence on the stability of the soil due to the configuration of the tests.
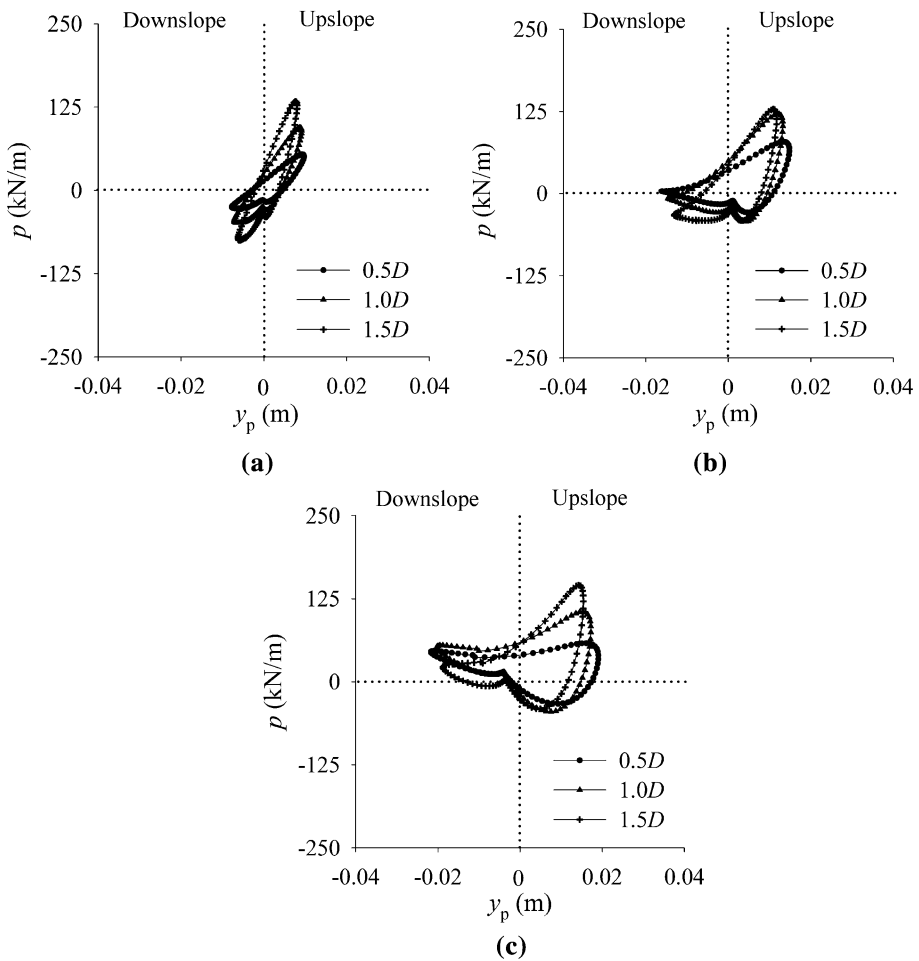
Fig. 11 Experimental dynamic $p–y_p$ loops at various depths (Model 2, $a_{base}=0.24g$). **a** Pile 1, **b** Pile 2, **c** Pile 3

4.3 Identification of unstable zone for slope case

As discussed, the area of the unstable zone of the soil mass for slope case might be identified by the shape of the $p–y_p$ loops, which have peak points in the second quadrant of the graph.

Figures 16 and 17 illustrate the prediction of soil mass that was unstable during shaking when the pile head moved in the downslope direction. In Model 2, the unstable zone of soil mass was expected to cover the area from the slope crest to some points near Pile 2, but did not reach the location of Pile 1, as shown in Fig. 16. This finding means that the slope effect on $p–y_p$ loops might decrease from the slope crest to the slope toe. The predicted depths of the unstable zone were about 0.25D, 0.5D, and 0.75D at Pile 2, and 1.5D, 1.7D, and 1.75D at Pile 3, corresponding to $a_{base}=0.14g$, 0.18g, and 0.24g, respectively. Below these predicted values, the slope effect on $p–y_p$ loops of three piles
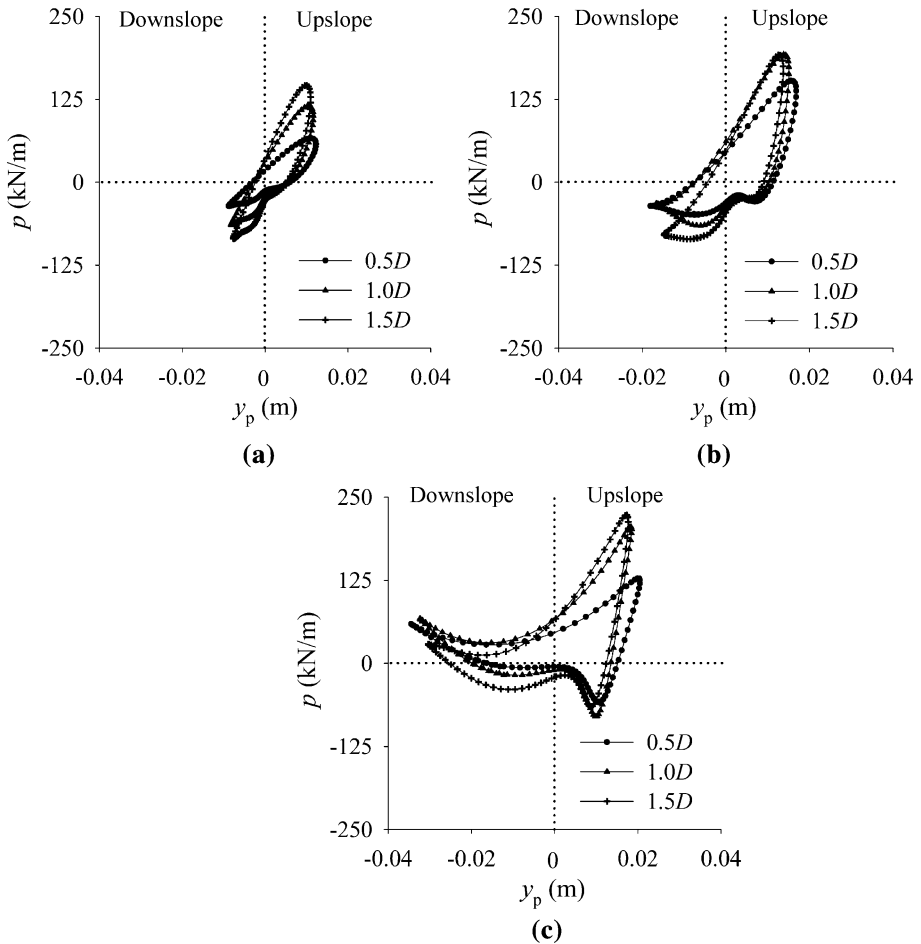
Fig. 12 Experimental dynamic p–y_p loops at various depths (Model 3, a_{base}=0.28g). **a** Pile 1, **b** Pile 2, **c** Pile 3

showed analogous behavior and thus the shape of lateral soil resistance distribution curves along the pile was almost similar behavior for all of three piles.

Figure 17 shows the typical lateral soil resistance in the downslope direction of Model 3. As the soil was denser, the area of the predicted unstable zone was reduced in comparison to Model 2. The predicted depths of the unstable zone were about 1.65D, 1.75D, and 1.85D at Pile 3 corresponding to a_{base} of 0.15g, 0.22g, and 0.28g, respectively.

The unstable zone might be significant for predicting the behavior of the lateral pile under dynamic conditions. Thus, the p–y curves in the unstable zone and lower zone need to be established for practical designs.
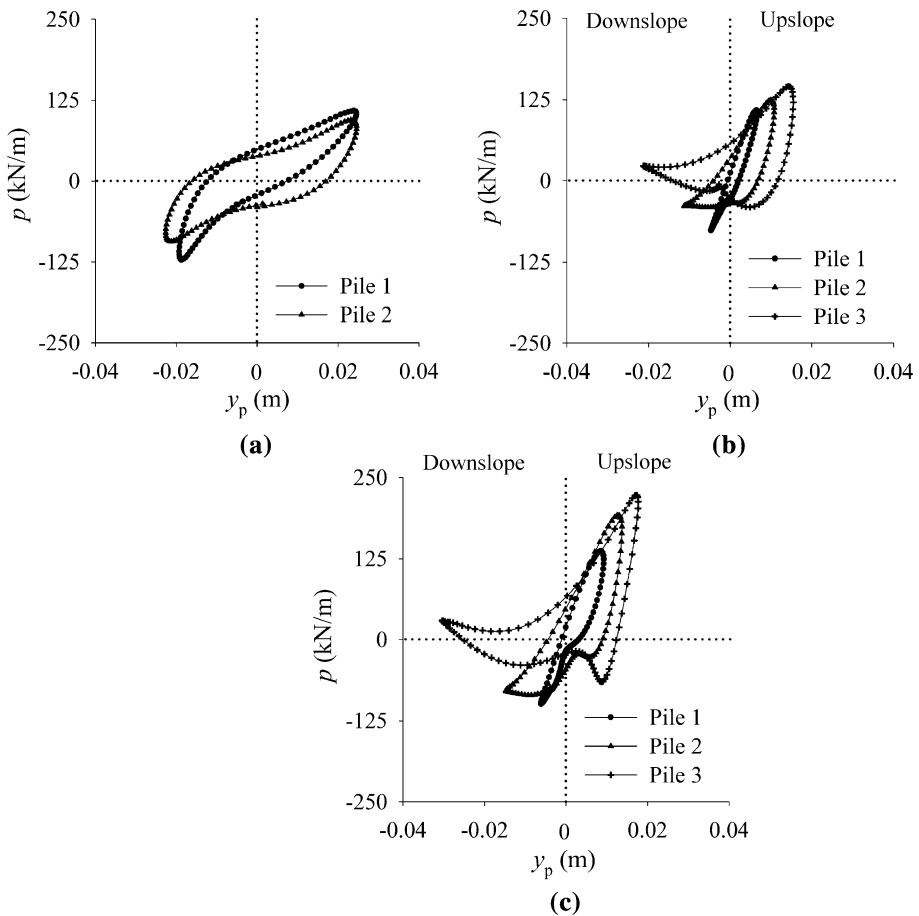
Fig. 13 Experimental dynamic p–y_p loops for three models (depth 1.5D). **a** Model 1 ($a_{base}=0.25g$), **b** Model 2 ($a_{base}=0.24g$), **c** Model 3 ($a_{base}=0.28g$)

4.4 p-multiplier for pile group

The p–y backbone curves of horizontal case in the present study were compared with those of API (2000) and Yoo et al. (2013) as shown in Figs. 18a, b. The comparison showed that the values of the ultimate lateral soil resistance of the API cyclic p–y curves were lower than those values from Yoo et al. (2013) and the present study. By contrast, the initial subgrade modulus of the API cyclic p–y curves was larger than that of Yoo et al. (2013) and the current study. Wilson (1998) also concluded that the ultimate lateral soil resistance of the API p–y curve underestimated that of the centrifuge tests at the shallow depth. In addition, the ultimate lateral soil resistance and initial subgrade modulus of p–y backbone curves from the present study were smaller than those of Yoo et al. (2013). The main reason for such differences was the effect of the pile group, i.e. Yoo et al. (2013) considered a single pile problem, whereas the present study was conducted on pile groups.

To obtain the p–y backbone curves of the piles in Model 1, the relative displacement between the soil and pile (y) was calculated by subtracting the soil displacement (y_s) from the
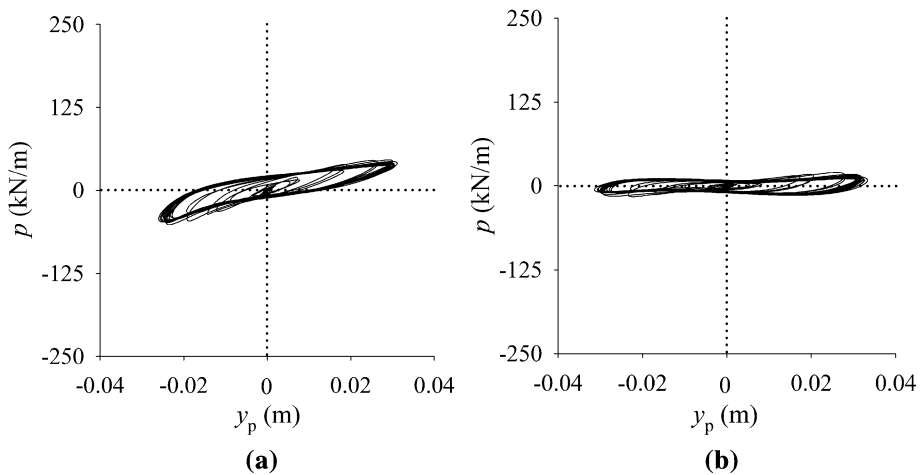
Fig. 14 Experimental dynamic p–y_p loops (Model 1, $a_{base} = 0.25g$). **a** Pile 1, 0.5D depth, **b** Pile 2, 0.25D depth

pile deflection (y_p). For each shaking level at each depth, the peak point of the experimental p–y loops was obtained and plotted on a p–y plane. To evaluate the effect of the pile group, a concept of p-multiplier suggested by Brown et al. (1988) was adopted. This concept was also extended to seismic loading in the previous studies such as Castelli and Maugeri (2009), Yang et al. (2010), and Yoo et al. (2012). The evaluation of the multiplier coefficients was processed through two steps. Firstly, the p–y curve of a single pile was calculated applying the formulas of the ultimate lateral soil resistance (p_u) and the subgrade reaction modulus (K) suggested by Yoo et al. (2013). Secondly, the multiplier coefficients imposed on p_u and K were obtained using the trial and error method to match the experimental results of pile groups of the present study.

The average multiplier coefficients applied for outer pile (Pile 1) were 0.766 and 0.656 for p_u and K, respectively. For center pile (Pile 2), the average coefficients were 0.728 and 0.592 for p_u and K, respectively. The multiplier coefficients of Pile 2 were slightly smaller than that of Pile 1 due to the shadowing effect. The same phenomenon was also found in previous studies under static condition (Mcvay et al. 1998; Christensen 2006; AASHTO 2012; Fayyazi et al. 2014). The AASHTO (2012) suggested p-multipliers for a 3×3 pile group with S/D of 5.0 as 1.0, 0.85, 0.7 for Rows 1, 2, and 3 (and higher), respectively. It was noticed that the p–multiplier for a pile group under a dynamic condition appeared smaller than that under a static condition. This disparity was due to the alternated roles of the outer piles (Piles 1 and 3) under seismic loading and the symmetry of the testing model. These predicted values might be applied to pile group installed in loose sand, which has an S/D of approximately 5.0. However, additional studies should be conducted with various pile spacing and frequencies of input motions to provide insights into the pile group effect.
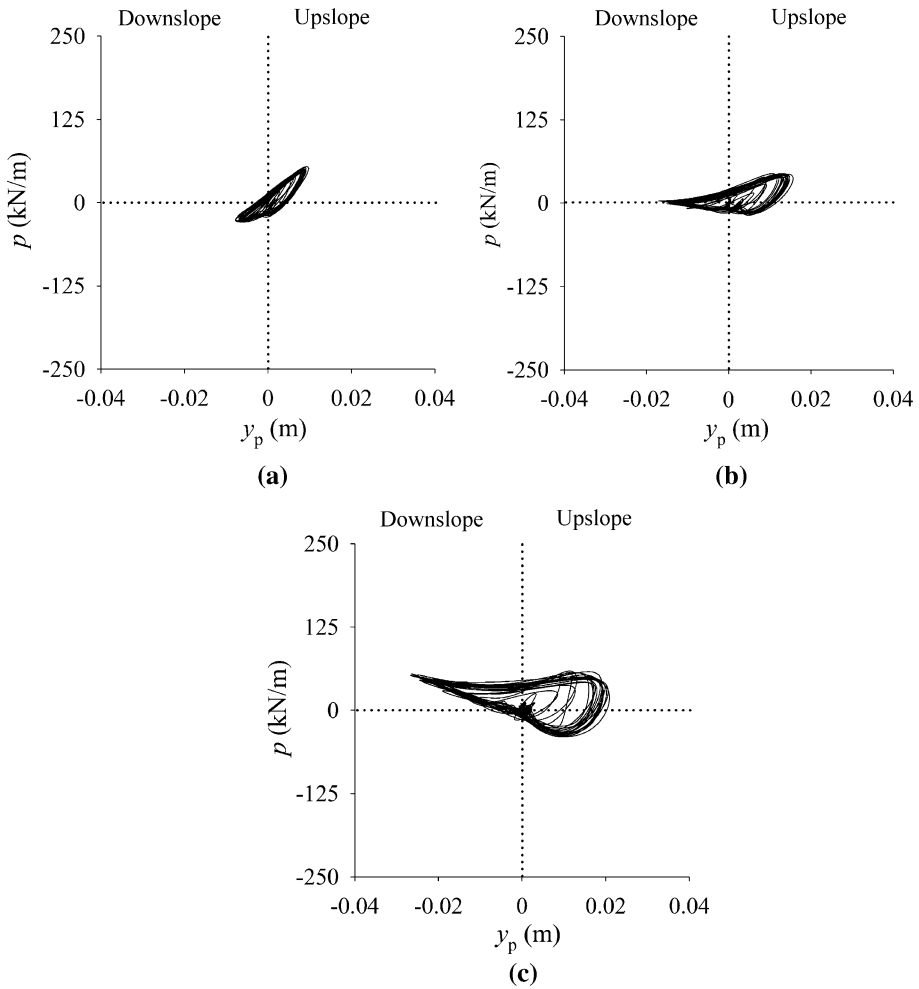
Fig. 15 Effect of slope on experimental dynamic p–y_p loops (Model 2, $a_{base}=0.24g$). **a** Pile 1, 0.5D depth, **b** Pile 2, 0.5D depth, **c** Pile 3, 0.5D depth

5 Conclusion

This study mainly addressed the slope effects on the seismic performance of pile-supported structures, particularly pile-supported wharves. A series of dynamic centrifuge tests were conducted, and the p–y_p loops were carefully evaluated to examine the dynamic soil–pile interaction in the sloping ground. The conclusions drawn from this study might be influenced by the present test conditions, such as the boundary effects of the ESB box and strain gauge distribution. Major conclusions can be summarized as follows:

1. In the slope cases, the depth of the maximum bending moment below ground surface in the downslope direction was deeper than that in the upslope direction. This phenomenon might occur because the passive soil resistance against the upslope pile movement was
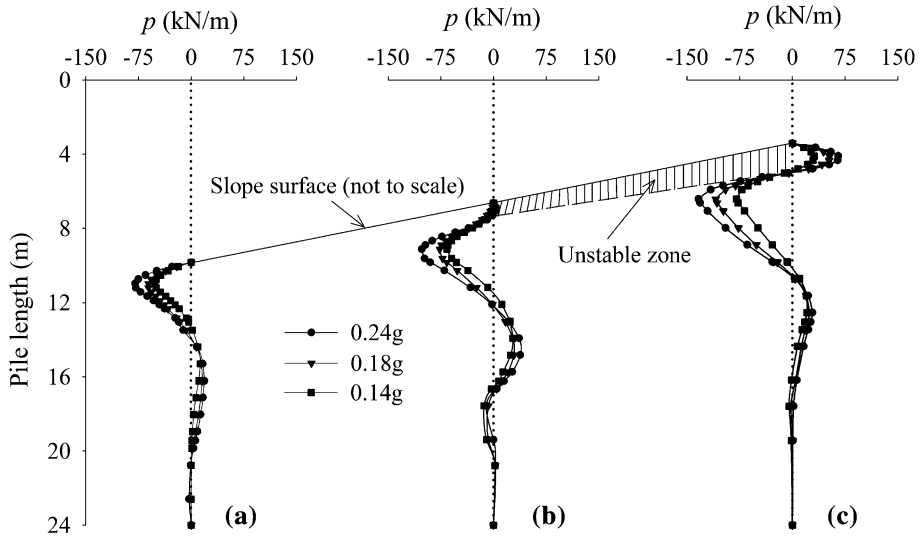
Fig. 16 Maximum lateral soil resistance distribution curves of Model 2. **a** Pile 1, **b** Pile 2, **c** Pile 3
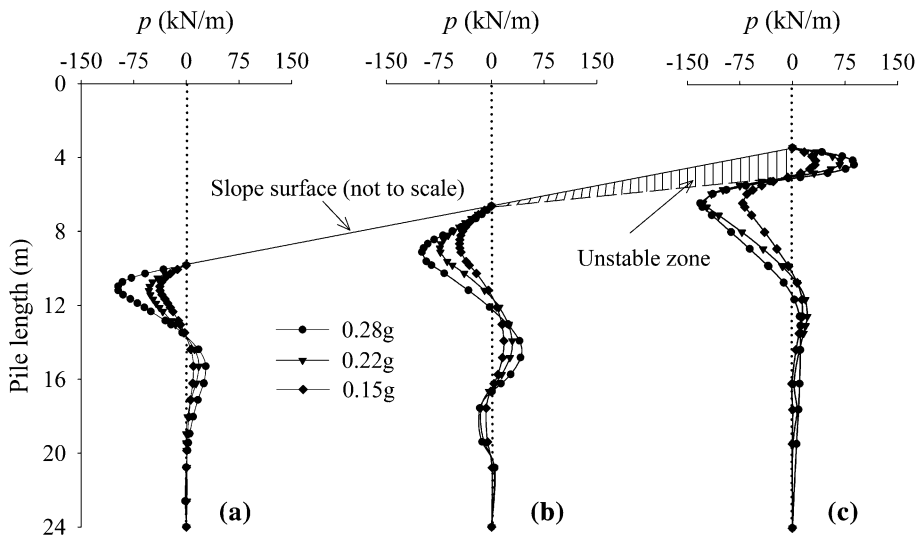

Fig. 17 Maximum lateral soil resistance distribution curves of Model 3. **a** Pile 1, **b** Pile 2, **c** Pile 3

larger than that against the downslope pile movement. In addition, the depth of the maximum moment was significantly changed according to the position of piles.

2. It was observed that the stiffness of the $p–y_p$ loops increased with depth according to the increase of the confining stress in the three models. Moreover, the stiffness and maximum lateral soil resistance of the $p–y_p$ loops in the slope cases were smaller in the downslope side than in the upslope side, whereas these properties were similar for both sides of the piles in the horizontal case.
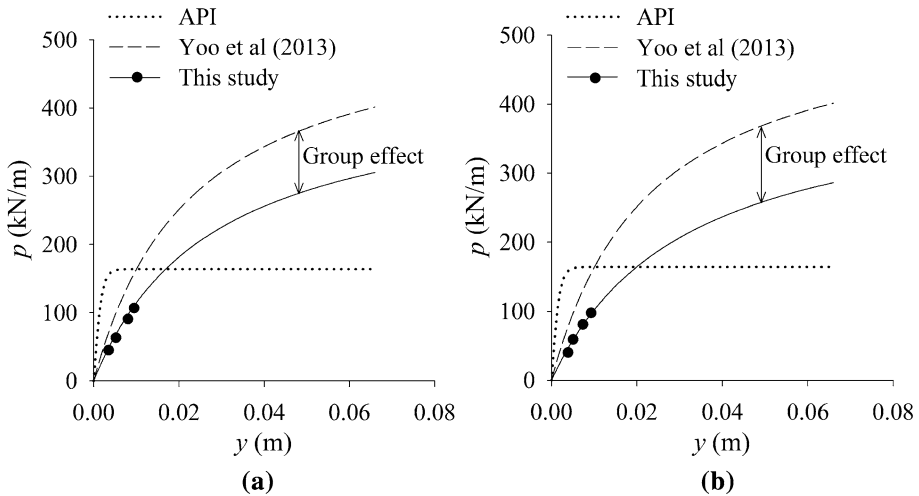
Fig. 18 Comparison of dynamic p–y backbone curve with existing p–y curves (Model 1, 1.5D depth). **a** Pile 1, **b** Pile 2

3. The p–y_p loops in the slope cases became stiffer from the crest to the toe of the slope. This phenomenon might be explained by the difference in unsupported length and earth pressure induced by slope configuration.

4. The unstable zone was determined by observing the irregular shape of the p–y_p loops. It was noticed that the area near the slope crest was the most unstable throughout shaking. Moreover, the unstable zone was reduced as the relative density of ground increased.

5. The group effect was evaluated for the piles in the horizontal ground. The proposed multiplier coefficients for the ultimate lateral soil resistance (p_u) and subgrade modulus (K) were 0.766 and 0.656, respectively, for the outer pile (Pile 1); and 0.728 and 0.592, respectively, for the center pile (Pile 2). These values might be applied for a pile group with S/D of about 5. Additional studies should be conducted with various pile spacing and frequencies of input motions to provide insights into the effects of the pile group.

References

AASHTO (2012) AASHTO LRFD Bridge design specifications, 6th edn. American Association of State Highway and Transportation Officials, Washington, DC

API (2000) Recommended practices for planning, designing and constructing fixed offshore platforms, API recommendation practice 2A (RP 2A), 21th edn. American Petroleum Institute, Washington, DC

American Society of Civil Engineers (ASCE) (2014) Seismic design of piers and wharves. *ASCE/COPRI 61-14*, USA

Bonab HM, Levacher D, Chazelas LJ, Kaynia MA (2014) Experimental study on the dynamic behavior of laterally loaded single pile. Soil Dyn Earthq Eng 66:157–166

Boulanger RW, Curras CJ, Kutter BL, Winson DW, Abghari A (1999) Seismic soil–pile-structure interaction experiments and analyses. J Geotech Geoenviron Eng 125(9):750–759

Brandenberg SJ, Boulanger RW, Kutter BL, Chang D (2005) Behavior of pile foundations in laterally spreading ground during centrifuge tests. J Geotech Geoenviron Eng 131(11):1378–1391

Brandenberg SJ, Wilson DW, Rashid M (2010) Weighted residual numerical differentiation algorithm applied to experimental bending moment data. J Geotech Geoenviron Eng 136(6):854–863

Brennan AJ, Thusyanthan NI, Madabhushi SP (2005) Evaluation of shear modulus and damping in dynamic centrifuge tests. J Geotech Geoenviron Eng 131(12):1488–1497

Brown D, Morrison C, Reese L (1988) Lateral load behavior of pile group in sand. J Geotech Geoenviron Eng 114(11):1261–1276

Castelli F, Maugeri M (2009) Simplified approach for the seismic response of a pile foundation. J Geotech Geoenviron Eng 135(10):1440–1451

Choi J, Kim M, Brandenberg SJ (2015) Cyclic $p–y$ plasticity model applied to pile foundations in sand. J Geotech Geoenviron Eng 141(5):04015013

Christensen S (2006) Full scale static lateral load test of a 9 pile group in sand. Master's thesis, Brigham Young University

Dou H (1991) Response of pile foundation under simulated earthquake loading. M.Sc. Thesis, University of British Columbia

Dou H, Byrne P (1996) Dynamic response of single piles and soil–pile interaction. Can Geotech J 33(1):80–96

El Naggar M, Bentley J (2000) Dynamic analysis for laterally loaded piles and dynamic $p–y$ curves. Can Geotech J 37(6):1166–1183

El Naggar M, Novak M (1995) Nonlinear lateral interaction in pile dynamic. Soil Dyn Earthq Eng 14:141–157

Fayyazi S, Taiebat M, Finn W (2014) Group reduction factors for analysis of laterally loaded pile groups. Can Geotech J 51:758–769

Georgiadis M, Anagnostopoulos C, Saflekou S (1992) Centrifugal testing of laterally loaded piles in sand. Can Geotech J 29:208–2016

Gerolymos N, Gazetas G (2005) Phenomenological model applied to inelastic response of soil–pile interaction systems. Soils Found 45(4):119–132

Gerolymos N, Escoffier S, Gazetas G, Garnier J (2009) Numerical modeling of centrifuge cyclic lateral pile load experiments. Earthq Eng Eng Vib 8(1):61–76

Haiderali AE, Madabhushi G (2016) Evaluation of curve fitting techniques in deriving $p–y$ curves for laterally loaded piles. Geotech Geol Eng 34(5):1453–1473

Khari M, Kassim KA, Adnan A (2014) Development of $p–y$ curves of laterally loaded piles in cohesionless soil. Sci World J 2014:917174

Kim DS, Kim NR, Choo YW, Cho GC (2013) A newly developed state-of-the-art geotechnical centrifuge in Korea. KSCE J Civ Eng 17(1):77–84

Kwon SY (2014) Numerical simulation of dynamic soil–pile-structure interactive behavior observed in centrifuge tests. PhD dissertation, Seoul National University

Lee SH, Choo YW, Kim DS (2012) Performance of an equivalent shear beam (ESB) model container for dynamic geotechnical centrifuge tests. Soil Dyn Earthq Eng 44:102–114

Madabhushi G (2014) Centrifuge modelling for civil engineering. CRC Press, London

MATLAB (2016) MATLAB version R2016a, a computer program. The Mathworks Inc., Natick

Matlock H (1970) Correlations for design of laterally loaded piles in soft clay. In: Proceeding of the 2nd annual offshore technology conference, vol 1, Houston, Texas, pp 577–594

McVay M, Casper R, Shang T (1998) Centrifuge testing of large laterally loaded pile groups in sands. J Geotech Geoenviron Eng 124(10):1016–1026

Mezazigh S, Levacher D (1998) Laterally loaded piles in sand: slope effect on $p–y$ reaction curves. Can Geotech J 35:433–441

Murchinson JM, O'Neill MW (1984) Elevation of $p–y$ relationships in cohesionless soils. In: Meyer JR (ed) Analysis design pile foundation. ASCE, New York, pp 174–191

Muthukkumaran K, Sundaravadivelu R, Gandhi RS (2008) Effect of slope on $p–y$ curves due to surcharge load. Soil Found 48(3):353–361

Nogami T, Otani J, Konagai K, Chen HL (1992) Nonlinear soil–pile interaction model for dynamic lateral motion. J Geotech Eng 18(1):89–106

OCDI (2009) Technical standards and commentaries for port and harbor facilities in Japan. The Overseas Coastal Area Development Institute of Japan, Tokyo

Reese LC, Cox WR, Koop FD (1974) Analysis of laterally loaded piles in sand. In: Proceedings of the 6th offshore technology conference, Paper 2080, Houston, Texas, pp 473–483

Rovithis E, Kirtas E, Pitilakis K (2009) Experimental *p–y* loops for estimating seismic soil–pile interaction. Bull Earthq Eng 7(3):719–736

Sivapriya SV, Gandhi SR (2011) Behavior of single pile in sloping ground under static lateral load. In: Proceeding of Indian geotechnical conference, pp 199–202

Ting JM, Kauffman CR, Lovicsek M (1987) Centrifuge static and dynamic lateral pile behavior. Can Geotech J 24:198–207

Varun (2010) A non-linear dynamic macroelement for soil structure interaction analyses of piles in liquefiable sites. Ph.D. Dissertation, Georgia Institute of Technology

Wilson DW (1998) Soil–pile-superstructure interaction in liquefying sand and soft clay. Ph.D. Dissertation, University of California at Davis

Wood DM (2004) Geotechnical modeling. Spon Press, New York

Yang K, Liang R (2006) Methods for deriving *p–y* curves from instrumented lateral load tests. GeotechTest J 30(1):31–38

Yang EK, Choi JI, Han JT, Kim MM (2010) Evaluation of dynamic group pile effect in sand by 1g shaking table tests. J Korea Geotech Soc 26(8):77–88 **(in Korean)**

Yang EK, Jeong S, Kim JH, Kim M (2011) Dynamic *p–y* backbone curves from 1g shaking table tests. KSCE J Civ Eng 15(5):813–821

Yoo MT, Cha SH, Kim MM, Choi JI, Han JT (2012) Evaluation of dynamic group-pile effect in dry sand by centrifuge model tests. INT J Offshore Polar 22(2):165–171

Yoo MT, Choi JI, Han JT, Kim MM (2013) Dynamic *p–y* curves for dry sand by dynamic centrifuge tests. J Earthq Eng 17(7):1082–1102